Desalination and Water Treatment
www.deswater.com
doi: 10.1080/19443994.2014.993717

57 (2016) 4371–4385
February

Oxazole derivatives as corrosion inhibitors for 316L stainless steel in sulfamic acid solutions

A.S. Fouda[a,*], M.A. Elmorsi[b], T. Fayed[b], I.A. El said[a]

[a]*Faculty of Science, Department of Chemistry, El-Mansoura University, El-Mansoura 35516, Egypt, Tel. +2 050 2365730; email: asfouda@hotmail.com (A.S. Fouda)*
[b]*Faculty of Science, Department of Chemistry, Tanta University, Tanta, Egypt, Tel. +2 040 3304824; email: melmorsy@hotmail.com (M.A. Elmorsi), tfayed@hotmail.com (T. Fayed)*

Received 2 May 2014; Accepted 18 November 2014

ABSTRACT

Oxazole derivatives were investigated as corrosion inhibitors for 316L stainless steel (SS) in sulfamic acid (NH_2HSO_3) solutions by potentiodynamic polarization, electrochemical impedance spectroscopy, and electrochemical frequency modulation techniques. The results showed the variation in inhibition performance of the inhibitors with varying concentrations and temperatures. The maximum efficiency was found to be 91% at 2×10^{-4} M concentration of the inhibitors for the immersion period of 3 h. Langmuir was tested to describe the adsorption behavior of inhibitor on 316LSS surface. Potentiodynamic polarization study clearly revealed that these compounds act as mixed-type inhibitors. The results of the electrochemical impedance study showed a decrease in double layer capacitance and increase in charge transfer resistance. The results of various electrochemical techniques show good agreements with each other.

Keywords: Corrosion inhibition; Stainless steel; Sulfamic acid; Potentiodynamic polarization; EIS; EFM

1. Introduction

Sulfamic acid (amido sulfuric acid) has long been used as an industrial cleaning agent due to its remarkable property of solubilizing hard scales and most of the deposits. Furthermore, it can be used on stainless steels with no problem of pitting or chloride-induced stress corrosion cracking (SCC). Sulfamic acid finds application in desalination plants for cleaning demisters, heat exchangers, and cooling water systems. Optimization in the sulfamic acid treatment is desirable in terms of plant efficiency and economic considerations. However, in spite of its capability as a potential descaling and an excellent cleaner, the industrial chemical treatment is somewhat qualitative due to the lack of corrosion and dissolution data regarding sulfamic acid [1]. Sulfamic acid behaves as a strong acid in aqueous solution but the corrosion rates are significantly lower in comparison to other acids [2]. The low corrosion rates can be reduced further by the addition of corrosion inhibitors [3]. It can be used for cleaning stainless steels with no problem of chloride-induced SCC. Due to these formidable properties, acid cleaners based on sulfamic acid are extensively used in a large variety of household and industrial applications [4].

---

*Corresponding author.

1944-3994/1944-3986

Efficient inhibitors for 316 SS are heterocyclic organic compounds consisting of a π-system and P, S, N, or O heteroatom [5]. It is noticed that the presence of these functional groups and heteroatom in the organic compound molecules improves its action as stainless steel corrosion inhibitor because they enable chemisorptions such as azoles [6–13], amines [14], amino acids [15], organic derivatives also offer special affinity to inhibit corrosion of various metals in different acidic media [16–26] and many others.

In this study, the various electrochemical techniques were used to investigate the effect of some oxazole derivatives as corrosion inhibitors for 316L SS in sulfamic acid solution.

2. Experimental

2.1. Composition of 316L SS samples

See Table 1.

2.2. Materials and solutions

Experiments were performed using 316L SS samples. These oxazole derivatives were synthesized as before [27]. The structures, names, molecular formulas and molecular weights of oxazole derivatives are shown in Table 2. The aggressive solution used was prepared by dilution of analytical reagent grade sulfamic acid with bidistilled water. The stock solution (1×10^{-2} M) of investigated compounds was used to prepare the desired concentrations by dilution with bidistilled water. The concentration range of investigated compounds was $4–20 \times 10^{-5}$ M.

2.3. Chemical measurements (weight loss measurements)

Six test pieces of 316L SS were cut into 2 × 2 × 0.2 cm. They were abraded with emery papers (a coarse paper was used initially and then progressively finer grades were employed), degreased in acetone, rinsed with bidistilled water, and finally dried between two filter papers and weighed. The test pieces were suspended by suitable glass hooks at the edge of the basin, and under the surface of the test solution by about 1 cm. Weight loss measurements were performed for 3 h at the temperature range from 25 to 55°C by immersing 316L SS pieces into 100 ml acid solution with and without various concentrations of inhibitors. After the specified period of time, the specimen were taken out of the test solution, rinsed with bidistilled water, dried as before, and weighed again accurately. The average weight loss at a certain time for each set of the six samples was taken. The weight loss was recorded to nearest 0.0001 g.

2.4. Electrochemical measurements

Electrochemical experiments were performed using a typical three-compartment glass cell consisted of the 316L SS specimen as working electrode (1 cm^2), saturated calomel electrode (SCE) as a reference electrode, and a platinum foil (1 cm^2) as a counter electrode. The reference electrode was connected to a Luggin capillary and the tip of the Luggin capillary is made very close to the surface of the working electrode to minimize IR drop. All measurements were done in solutions open to atmosphere under unstirred conditions. All potential values were reported vs. SCE. Prior to every experiment, the electrode was abraded with successive different grades of emery paper, degreased with acetone and washed with bidistilled water, and finally dried. Tafel polarization curves were obtained by changing the electrode potential automatically from (−1.0 to 0.2 V vs. SCE) at open-circuit potential with a scan rate of 1 mVs^{-1}. The corrosion current is performed by extrapolation of anodic and cathodic Tafel lines to a point which gives log i_{corr} and the corresponding corrosion potential (E_{corr}) for inhibitor free acid and for each concentration of inhibitor.

Impedance measurements were carried out in frequency range from 100 kHz to 0.1 Hz with amplitude of 5 mV peak-to-peak using ac signals at open-circuit potential. Before measurements, the electrode was immersed in solution for 30 min until a steady state was reached. The experimental impedance was analyzed and interpreted based on the equivalent circuit. The main parameters deduced from the analysis of Nyquist diagram are the charge transfer resistance R_{ct} (diameter of high-frequency loop) and the double layer capacity C_{dl}.

Table 1
Chemical composition of 316L SS in wt.%

Element	C	Cr	Ni	Mo	Mn	Si	P	S	N	Fe
Wt.%	0.03	16–18	10–14	2–3	2	0.75	0.045	0.03	0.1	Balance

Electrochemical frequency modulation (EFM) was carried out using two frequencies 2 and 5 Hz. The base frequency was 0.1 Hz, so the waveform repeats after 1 s. The higher frequency must be at least two times the lower one. The higher frequency must also be sufficiently slow that the charging of the double layer does not contribute to the current response. Often, 10 Hz is a reasonable limit. The intermodulation spectra contain current responses assigned for harmonical and intermodulation current peaks. The larger peaks were used to calculate the corrosion current density (i_{corr}), the Tafel slopes (β_c and β_a), and the causality factors CF-2 & CF-3.

All electrochemical measurements were performed using Gamry Instrument (PCI 300/4) Potentiostat/Galvanostat/ZRA. This includes a Gamry framework system based on the ESA 400. Gamry applications include DC105 software for potentiodynamic polarization, EIS300 software for electrochemical impedance spectroscopy and EFM 140 software for EFM measurements along with a computer for collecting data. Echem Analyst 6.03 software was used for plotting, graphing, and fitting data.

To test the reliability and reproducibility of the measurements, duplicate experiments were performed in each case at the same conditions.

3. Results and discussion

3.1. Weight loss method

Fig. 1 shows plots for the variation of weight loss of 316L SS with time for the corrosion of 316L SS in 0.6 M NH_2HSO_3 containing various concentrations of compound (*D*) at 25˚C. Similar curves were obtained for other inhibitors but not shown. From the plots, it is evident that the weight loss of SS was also found to decrease with increase in the concentration of compound (*D*). The weight loss of SS in the blank solution was also found to be higher than those obtained for solutions of NH_2HSO_3 containing various concentrations of compound (*D*). This indicates that compound *D* is an adsorption inhibitor for the corrosion of SS in solutions of NH_2HSO_3. In Table 3, values of the corrosion rates of 316L SS and inhibition efficiency of all studied compounds in various media are presented. The degree of surface coverage (θ) and inhibition efficiency (% IE) were calculated using Eq. (1):

$$\% \text{ IE} = \theta \times 100 = [1 - \text{CR}_{\text{inh}}/\text{CR}_{\text{free}}] \times 100 \quad (1)$$

where CR_{inh} and CR_{free} are the corrosion rates in the absence and presence of inhibitor, respectively. It can

Table 2
Chemical structures, names, molecular weights, and molecular formulas of oxazole derivatives

Inhibitor	Structures	Names	Molecular weights	Chemical formulas
A	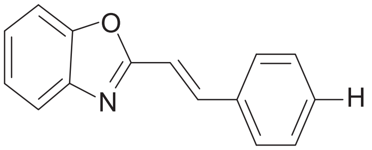	(E)-2-styrylbenzo[d]oxazole	221.25	$C_{15}H_{11}NO$
B	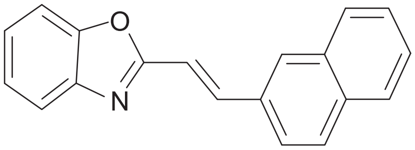	E)-2-(2-(naphthalene-2-yl)vinyl) benzo[d]oxazole	271.31	$C_{19}H_{13}NO$
C	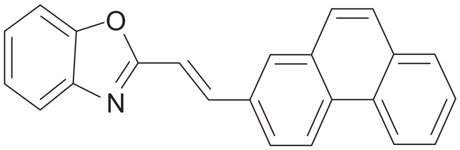	(E)-2-(2-(phenanthren-2-yl)vinyl) benzo[d] oxazole	321.37	$C_{23}H_{15}NO$
D	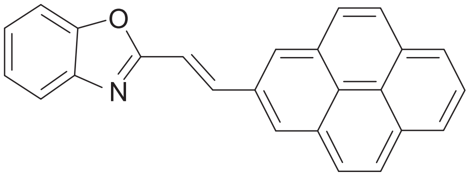	(E)-2-(2-(pyren-2-yl)vinyl)benzo[d] oxazole	345.39	$C_{25}H_{15}NO$

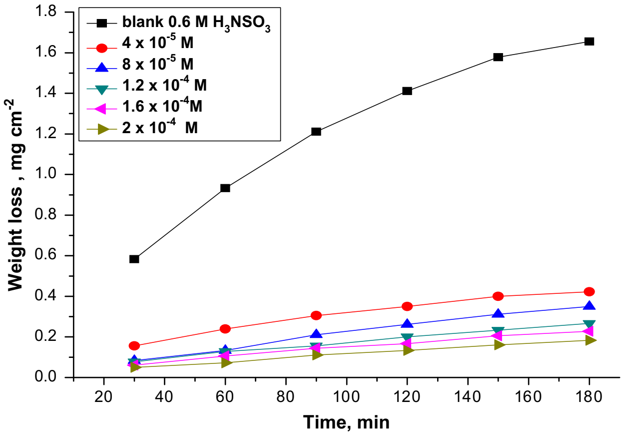

Fig. 1. Weight loss-time curves for the corrosion of 316L SS in 0.6 M NH_2HSO_3 in the absence and presence of different concentrations of inhibitor (*D*) at 25˚C.

be seen that the maximum of 90.6% inhibition efficiency is achieved at 2×10^{-4} M of inhibitor concentration and % IE increases with increasing the inhibitor concentrations [26]. This is mainly due to the active chemical constituent of viz, π bonds, hetero atoms (O and N). The almost greater than 90% of surface coverage (θ) is due to the co-ordination between the metal and the hetero atom present in the inhibitor. From the calculated values of % IE, the order of the inhibition efficiency of inhibitors was as follows: D > B > A > C.

3.2. Effect of temperature on inhibition efficiency (% IE)

The inhibition efficiency (% IE) for 316L SS corrosion in the presence of various concentrations of the investigated oxazole derivatives and at different temperatures was calculated and is listed in Table 4. The results of Table 4 illustrate the variation of corrosion rate (CR) and % IE with inhibitor concentrations at different temperatures. The obtained data revealed that the inhibition efficiency decreased with an increase in the inhibitor concentration. This suggests that the inhibitor species are adsorbed on the 316L SS/solution interface where the adsorbed species mechanically form a protected film on the metal surface which inhibits the action of the corrosion. A close comparison between Tables 2 and 3 revealed that weight loss of SS increases with increasing temperature indicating that the rate of corrosion of SS increases with increase in temperature. The value of inhibition efficiency was decreased with rise in temperature suggesting physical adsorption mechanism [28]. These results indicate that the adsorption of investigated compounds shield the metal surface at room temperature [29]. However, it may be deshielded from the surface with rise in temperature. It is also clear that corrosion rate of 316L SS in the absence and presence of inhibitors obey Arrhenius type equation as it increases with raising solution temperature. The dependence of corrosion rate (k_{corr}) on the temperature can be expressed by Arrhenius Eq. (2):

$$i_{\text{corr}}(k_{\text{corr}}) = A \exp\left(-E_{\text{a}}^*/RT\right) \quad (2)$$

where A is the pre-exponential factor and E_{a}^* is the apparent activation energy of the corrosion process. Arrhenius plot obtained for the corrosion of carbon steel in 0.5 M sulfamic acid solutions in the presence of different concentrations of compound (*D*) is shown in Fig. 2. E_{a}^* values determined from the slopes of these linear plots are shown in Table 5. The linear regression (R^2) is close to 1 which indicates that the corrosion of 316L SS in 0.5 M sulfamic acid solutions can be elucidated using the kinetic model. Table 5 showed that the values of E_{a}^* for inhibited solution is higher than that for uninhibited solution, suggesting that dissolution of 316L SS is slow in the presence of inhibitor. It is known from Eq. (2) that the higher E_{a}^*

Table 3
Corrosion rate (k_{corr}) and inhibition efficiency (% IE) at different concentrations of inhibitors for the corrosion of 316L SS after 120 min immersion in 0.6 M NH_2HSO_3 at 25˚C

	A		B		C		D	
Conc. × 10^5, M	$k_{\text{corr}} \times 10^{-3}$, mg cm^{-2} min^{-1}	% IE	$k_{\text{corr}} \times 10^{-3}$, mg cm^{-2} min^{-1}	% IE	$k_{\text{corr}} \times 10^{-3}$, mg cm^{-2} min^{-1}	% IE	$k_{\text{corr}} \times 10^{-3}$, mg cm^{-2} min^{-1}	% IE
4.0	3.24	72.4	3.47	70.5	4.07	65.4	2.91	75.2
8.0	2.63	77.6	2.82	76.0	3.28	72.0	2.17	81.5
12	2.12	81.9	2.12	81.9	2.59	78.0	1.66	85.8
16	1.66	85.8	1.43	87.8	2.17	81.5	1.38	88.2
20	1.48	87.4	1.25	89.4	1.89	83.9	1.11	90.6

Table 4
Variation of inhibition efficiency (% IE) and corrosion rate (k_{corr}) for various concentrations of the studied inhibitors at different temperatures

		A		B		C		D	
Temp., °C	Conc. × 10^5, M	$k_{corr} \times 10^{-3}$, mg cm^{-2} min^{-1}	% IE	$k_{corr} \times 10^{-3}$, mg cm^{-2} min^{-1}	% IE	$k_{corr} \times 10^{-3}$, mg cm^{-2} min^{-1}	% IE	$k_{corr} \times 10^{-3}$, mg cm^{-2} min^{-1}	% IE
35	4	8.28	66.5	8.05	67.5	9.02	63.5	7.407	70.1
	8	6.66	73.1	6.57	73.5	7.59	69.3	5.324	78.5
	12	5.23	78.9	5.32	78.5	6.43	74.0	3.98	83.9
	16	4.62	81.3	3.98	83.9	5.41	78.1	3.37	86.4
	20	3.75	84.9	2.91	88.2	4.58	81.5	2.73	89.0
45	4	17.87	65.3	17.68	65.6	18.84	63.4	15.55	69.8
	8	14.72	71.4	15.00	70.9	17.26	66.5	11.48	77.7
	12	12.17	76.3	12.08	76.5	14.63	71.5	8.70	83.1
	16	10.41	79.8	8.51	83.5	12.54	75.6	7.59	85.3
	20	9.35	81.8	7.45	85.5	10.92	78.8	6.20	88.0
55	4	37.31	63.3	38.05	62.5	44.30	65.4	31.29	69.2
	8	31.11	69.4	32.22	68.3	36.08	63.8	24.21	76.2
	12	26.34	74.1	26.11	74.3	31.20	69.3	19.07	81.2
	16	23.75	76.6	19.02	81.3	26.89	73.5	16.20	84.0
	20	21.76	78.6	16.29	83.9	24.21	76.2	13.28	78.0

values lead to the lower corrosion rate. This is due to the formation of a film on the carbon steel surface serving as an energy barrier for the carbon steel corrosion [30].

Enthalpy and entropy of activation (ΔH^*, ΔS^*) of the corrosion process were calculated from the transition state theory as given from Eq. (3) (Table 5):

$$k_{corr} = (RT/Nh)\exp(\Delta S^*/R)\exp(-\Delta H^*/RT) \quad (3)$$

where h is the Planck's constant and N is the Avogadro's number. A plot of log (k_{corr}/T) vs. $1/T$ for carbon steel in 0.5 M sulfamic acid with different concentrations of compound (*D*) gives straight lines as shown in Fig. 3. Similar curves were obtained for other compounds but not shown. Values of ΔH^* are positive. This indicates that the corrosion process is an endothermic one. The entropy of activation ΔS^* is large and negative. This implies that the activated complex represents association rather than dissociation

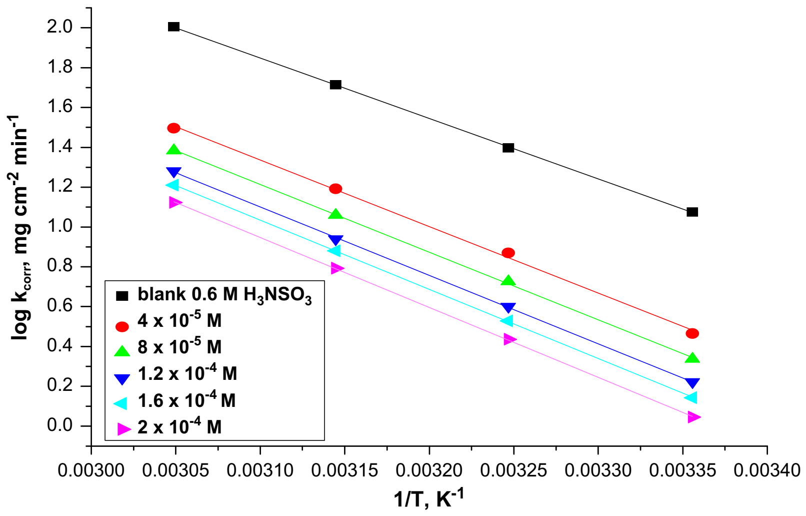

Fig. 2. Arrhenius plots for 316L SS rates (k_{corr}) after 120 min immersion in 0.6 M H_2NHSO_3 in the absence and presence of various concentrations of inhibitor (*D*).

Table 5
Activation parameters for 316L SS surface corrosion in the absence and presence of various concentrations of investigated inhibitors in 0.6 M H_2NHSO_3

		Activation parameters		
Inhibitor	Conc. × 10^5, M	$-E^*_a$, kJ mol^{-1}	ΔH^*, kJ mol^{-1}	$-\Delta S^*$, J mol^{-1} K^{-1}
Blank	0.0	58.1	55.9	36.9
A	4	65.9	63.3	22.5
	8	66.6	64.0	21.7
	12	68.2	65.6	18.4
	16	71.4	68.8	9.4
	20	72.9	70.3	5.7
B	4	64.7	62.1	26.0
	8	66.0	63.4	23.4
	12	67.8	65.6	18.4
	16	69.2	66.7	17.8
	20	70.2	67.6	16.3
C	4	64.1	61.5	27.1
	8	65.6	63.0	23.7
	12	67.1	64.8	19.5
	16	68.2	65.6	18.3
	20	69.1	66.5	16.4
D	4	64.0	61.4	29.7
	8	65.0	62.4	28.8
	12	65.8	63.2	28.6
	16	66.5	63.9	27.6
	20	67.2	64.6	27.2

step, indicating that a decrease in disorder takes place, going from reactants to the activated complex [31].

3.3. Adsorption isotherms

Adsorption isotherm values are important to explain the mechanism of corrosion inhibition of organo-electrochemical reactions. The most frequently used isotherms are Langmuir isotherm (Fig. 4). Thermodynamic parameters for the adsorption of different inhibitors on 316L SS surface in 0.6 M H_2NHSO_3 at different temperatures was listed in Table 6. From Table 6 it was found that: the negative values of ΔG°_{ads} reflect that the adsorption of studied oxazole derivatives on 316L SS in 0.6 M H_2NHSO_3 solution is a spontaneous process [32]. ΔG°_{ads} values increase (become less negative) with an increase in temperature which indicates the occurrence of exothermic process at which adsorption was unfavorable with increasing reaction temperature as the result of the inhibitor desorption from the stainless steel surface [33]. It is usually accepted that the value of ΔG°_{ads} around −20 kJ mol^{-1} or lower indicates the electrostatic interaction between charged metal surface and charged organic molecules in the bulk of the solution [34]. The negative sign of ΔH°_{ads} reveals that the adsorption of inhibitor molecules is an exothermic process. Generally, an exothermic adsorption process suggests either physisorption or chemisorption while endothermic process is attributed to

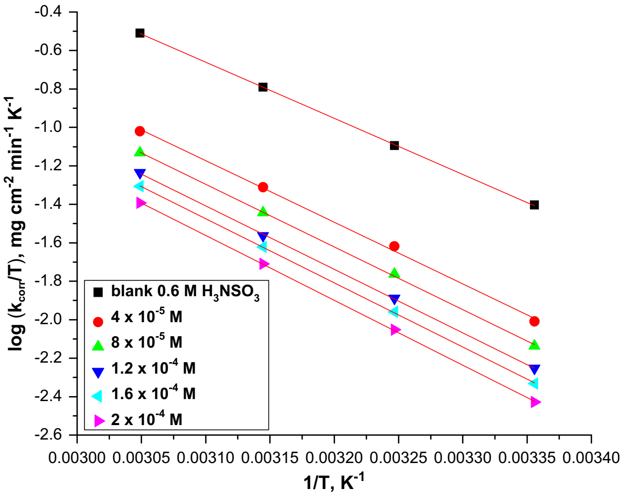

Fig. 3. Transition state plots for 316L SS (k_{corr}/T vs. $1/T$) after 120 min immersion in 0.6 M H_2NHSO_3 in the absence and presence of various concentrations of compound (*D*).

Table 6
Thermodynamic adsorption parameters for the adsorption of oxazole derivatives on 316L SS in 0.6 M sulfamic acid at different temperatures

Inhibitor	Temp., ˚C	K_{ads}, M^{-1}	$-\Delta G^{\circ}_{ads}$, kJ mol^{-1}	$-\Delta H^{\circ}_{ads}$, kJ mol^{-1}	$-\Delta S^{\circ}_{ads}$, J mol^{-1} K^{-1}
A	25	28.04	18.21	22.38	61.04
	35	22.16	18.22	22.38	59.09
	45	16.73	18.07	22.38	56.75
	55	12.26	17.79	22.38	54.17
B	25	40.18	19.10	15.16	64.06
	35	33.22	19.25	15.16	62.48
	45	26.51	19.29	15.16	60.60
	55	23.28	19.53	15.16	59.53
C	25	21.11	17.51	15.91	58.70
	35	16.58	17.48	15.91	56.70
	45	12.70	17.34	15.91	54.48
	55	12.05	17.74	15.91	54.04
D	25	40.42	19.12	10.81	64.12
	35	35.31	19.42	10.81	63.00
	45	30.70	19.68	10.81	61.84
	55	27.18	19.96	10.81	60.83

chemisorptions [35]. Generally, enthalpy values up to 41.9 kJ mol^{-1} are related to the electrostatic interactions between charged molecules and charged metal (physisorption) while those around 100 kJ mol^{-1} or higher are attributed to chemisorption. The unshared electron pairs in investigated molecules may interact with d-orbitals of Fe to provide a protective chemisorbed film [36]. In the case of investigated compounds, the absolute values of enthalpy are relatively low, approaching those typical of physisorption. The values of ΔS°_{ads} in the presence of investigated compounds are large and negative that is accompanied with exothermic adsorption process. [37]. The experimental data give good curves fitting for the applied adsorption isotherm as the correlation coefficients (R^2) were in the range 0.950–0.997. K_{ads} value decreases with the increase in temperature from 25 to 55˚C (Fig. 5).

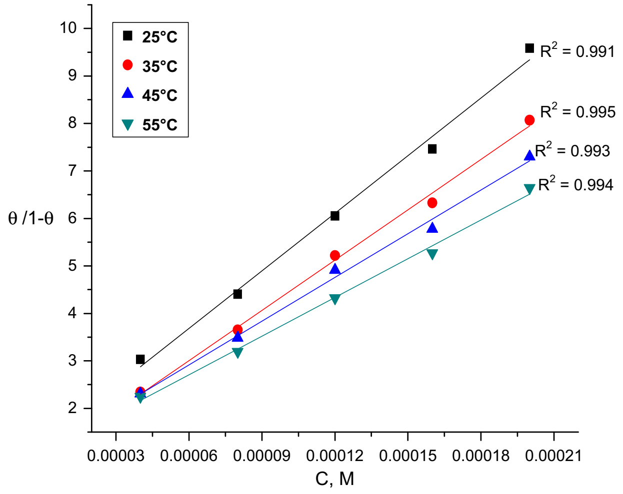

Fig. 4. Langmuir adsorption isotherm of inhibitor (*D*) on 316L SS in 0.6 M H_2NHSO_3 at different temperatures.

3.4. Potentiodynamic polarization measurements

Polarization measurements were carried out in order to gain knowledge concerning the kinetics of the cathodic and anodic reactions. Fig. 6 presents the results of the effect of compound (*D*) on the cathodic and anodic polarization curves of 316L SS in 0.6 M H_2NHSO_3. Similar curves for other compounds were obtained but not shown. It could be observed that both the cathodic and anodic reactions were suppressed with the addition of investigated compounds, which suggested that these compounds reduced anodic dissolution and also retarded the hydrogen evolution reaction. Electrochemical corrosion kinetics parameters, i.e. corrosion potential (E_{corr}), cathodic and anodic Tafel slopes (β_a, β_c), and corrosion current density (i_{corr}) obtained from the extrapolation of the polarization curves, were given in Table 7. The parallel cathodic Tafel curves in Fig. 6 suggested that the hydrogen evolution is activation-controlled and the reduction mechanism is not affected by the presence of the inhibitor. The region between linear part of cathodic and anodic branch of polarization curves becomes wider as the inhibitor is added to the acid

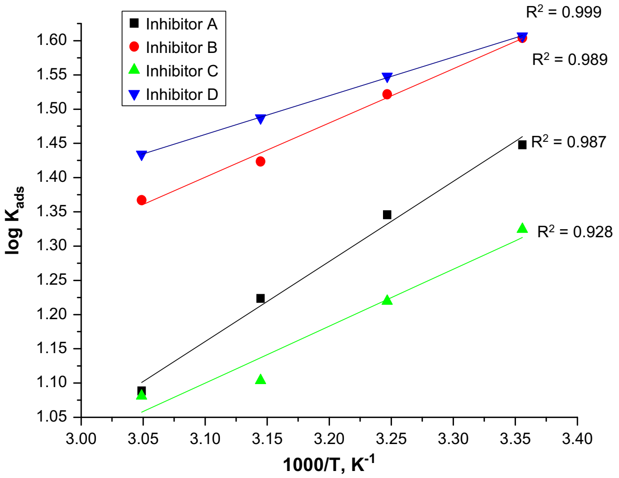

Fig. 5. (log K_{ads}) vs. (1/T) for the corrosion of 316L SS in 0.6 M H_2NHSO_3 in the presence of different inhibitors.

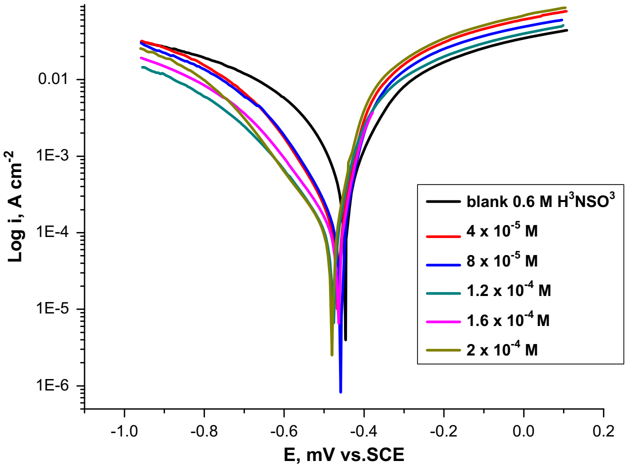

Fig. 6. Potentiodynamic polarization curves for the dissolution of 316L SS in 0.6 M H_2NHSO_3 in the absence and presence of different concentrations of compound (D) at 25°C.

solution. Similar results were found in the literature [38]. The values of β_a and β_c changed slightly with increasing inhibitor concentration indicated the influence of these compounds on the kinetics of metal dissolution and of hydrogen evolution. Due to the presence of some active sites, such as aromatic rings, hetero-atoms in the studied compound for making adsorption, they may act as adsorption inhibitors. Being absorbed on the metal surface, these compounds controlled the anodic and cathodic reactions during corrosion process, and then their corrosion inhibition efficiencies are directly proportional to the amount of adsorbed inhibitor. The functional groups and structure of the inhibitor play important roles during the adsorption process. On the other hand, an electron transfer takes place during adsorption of the neutral organic compounds at metal surface [39]. As it can be seen from Table 7, the studied inhibitors reduced both anodic and cathodic currents with a slight shift in corrosion potential (47 mV). According to Ferreira and others [40], if the displacement in corrosion potential is more than 85 mV with respect to corrosion potential of the blank solution, the inhibitor can be seen as a cathodic or anodic type. In the present study, the displacement was 47 mV which indicated that the studied inhibitor is mixed-type inhibitor. The results obtained from Tafel polarization showed good agreement with the results obtained from weight loss method. The surface coverage (θ) and % IE were calculated using Eq. (4):

$$\% \text{ IE} = \theta \times 100 = [1 - (i_{\text{corr}}/i^{\circ}_{\text{corr}})] \times 100 \qquad (4)$$

where i_{corr} and i°_{corr} are the current densities in presence and absence of inhibitor, respectively.

3.5. Electrochemical impedance spectroscopy measurements

Nyquist plots of 316L SS in uninhibited and inhibited acid solutions containing different concentrations of compound (D) are presented in Fig. 7. Electrochemical impedance spectroscopy (EIS) spectra obtained consists of one depressed capacitive loop (one time constant in Bode-phase plot). The increased diameter of capacitive loop obtained in 0.6 M H_2NHSO_3 in presence of compound (D) indicated the inhibition of corrosion of 316L SS. The high frequency capacitive loop may be attributed to the charge transfer reaction. Corrosion kinetic parameters derived from EIS measurements and inhibition efficiencies are given in Table 8. Double layer capacitance (C_{dl}) and charge transfer resistance (R_{ct}) were obtained from EIS measurements as described elsewhere [41]. It is apparent from Table 7 that the impedance of the inhibited system amplified with the inhibitor the C_{dl} values decreased with inhibitor. This decrease in C_{dl} results from a decrease in local dielectric constant and/or an increase in the thickness of the double layer, suggested that inhibitor molecules inhibit the iron corrosion by adsorption at the metal/acid interface [42]. The depression in Nyquist semicircles is a feature for solid electrodes and often referred to as frequency dispersion and attributed to the roughness and other in homogeneities of the solid electrode [43]. In this behavior of solid electrodes, the parallel network: charge transfer

Table 7
Effect of concentrations of various compounds on the free corrosion potential (E_{corr}), corrosion current density (i_{corr}), Tafel slopes ($\beta_c \beta_a$), corrosion rate (k_{corr}), degree of surface coverage (θ), and inhibition efficiency (% IE) of 316L SS in (0.6 M) H_2NHSO_3

Inh	[Inh] × 10^5, M	$-E_{corr}$, mV vs SCE	i_{corr}, μA cm^{-2}	β_c, mV dec^{-1}	β_a, mV dec^{-1}	k_{corr}, mmy^{-1}	θ	% IE
Blank	0.0	446	1,160	241	186	1,064	–	–
A	4	433	475	179	109	433.9	0.591	59.1
	8	474	261	282	144	238.1	0.775	77.5
	12	480	191	202	107	174.6	0.835	83.5
	16	465	131	150	56	120.1	0.887	88.7
	20	466	95.4	135	53	87.2	0.918	91.8
B	4	436	362	186	107	330.6	0.688	68.8
	8	456	233	176	88	212.8	0.799	79.9
	12	457	189.0	184	79	172.9	0.837	83.7
	16	463	131.0	180	78	119.3	0.887	88.7
	20	477	93.6	145	49	85.5	0.919	91.9
C	4	448	500.0	109	83	457.4	0.569	56.9
	8	460	272.0	225	114	248.9	0.766	76.6
	12	473	192.0	205	93	175.9	0.834	83.4
	16	464	126.0	163	55	114.9	0.891	89.1
	20	472	106.0	147	54	97.0	0.909	90.9
D	4	466	292.0	190	97	266.6	0.748	74.8
	8	459	206.0	162	83	188.4	0.822	82.2
	12	475	159.0	202	79	144.9	0.863	86.3
	16	464	126.0	163	55	114.9	0.891	89.1
	20	480	91.0	141	46	83.2	0.922	92.2

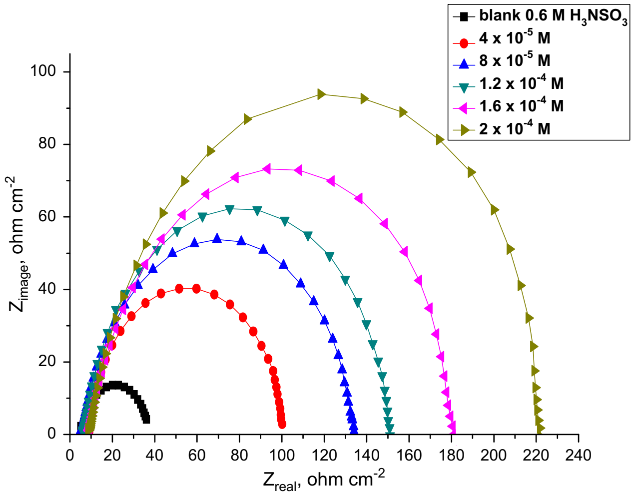

Fig. 7. The Nyquist plots for the corrosion of 316L SS in 0.6 M H_2NHSO_3 in the absence and presence of different concentrations of compound (*D*) at 25°C.

resistance-double layer capacitance is established where an inhibitor is present. For the description of a frequency independent phase shift between an applied ac potential and its current response, a constant phase element (CPE) is used which is defined in impedance representation as in Eq. (5)

$$Z_{CPE} = Y_o^{-1}(i\omega)^{-n} \tag{5}$$

where Y_o is the CPE constant, ω is the angular frequency (in rad s^{-1}), $i^2 = -1$ is the imaginary number, and n is a CPE exponent which can be used as a gauge of the heterogeneity or roughness of the surface [44]. Depending on the value of n, CPE can represent resistance ($n = 0$, $Y_o = R$), capacitance ($n = 1$, $Y_o = C$), inductance ($n = -1$, $Y_o = L$), or Warburg impedance ($n = 0.5$, $Y_o = W$).

Fig. 8 showed the electrical equivalent circuit employed to analyze the impedance spectra. Excellent fit with this model was obtained for all experimental data. The surface coverage (θ) and % IE were calculated using Eq. (6):

$$\% \text{ IE} = \theta \times 100 = [1 - (R_{ct}/R^{\circ}_{ctcorr})] \times 100 \tag{6}$$

where R_{ct} and R°_{ct} are the charge transfer resistances in absence and presence of inhibitor, respectively.

The results obtained from weight loss, potentiodynamic polarization, and impedance techniques are in a good agreement but it is of interest to note that, the

Table 8
EIS parameters for the corrosion of 316L SS in 0.6 M H_2NHSO_3 in the absence and presence of different concentrations of investigated compound at 25˚C

Inhibitor	Conc. × 10^5, M	C_{dl}, μF cm^{-2}	R_{ct}, Ω cm^2	θ	% IE
Blank	0.0	452.33	31.57	–	–
A	4	91.23	66.61	0.52	52.6
	8	85.02	124.0	0.74	74.5
	12	53.84	128.8	0.75	75.5
	16	47.18	163.4	0.80	80.7
	20	45.98	200.5	0.84	84.3
B	4	305.47	72.28	0.563	56.3
	8	237.07	117.50	0.731	73.1
	12	109.09	140.00	0.775	77.5
	16	90.75	172.00	0.816	81.6
	20	75.10	210.00	0.850	85.0
C	4	116.72	37.46	0.157	15.7
	8	92.14	116.40	0.729	72.9
	12	90.09	135.00	0.766	76.6
	16	84.88	177.20	0.822	82.2
	20	80.07	206.10	0.847	84.7
D	4	107.07	92.41	0.658	65.8
	8	93.15	130.70	0.758	75.8
	12	90.61	147.20	0.786	78.6
	16	72.99	178.80	0.823	82.3
	20	67.93	224.70	0.860	86.0

values of % IE given by electrochemical techniques are higher than those obtained by weight loss measurements; this may be due to the fact that the electrochemical measurements were carried out on freshly prepared solutions.

3.6. EFM measurements

EFM is a nondestructive corrosion measurement like EIS, it is a small signal ac technique. Unlike EIS, however, two sine waves (at different frequencies) are applied to the cell simultaneously. The great strength of the EFM is the causality factors which serve as an internal check on the validity of the EFM measurement [45]. With the causality factors, the experimental EFM data can be verified. The results of EFM experiments are a spectrum of current response as a function of frequency. The spectrum is called the intermodulation spectrum. The spectra contain current responses assigned for harmonical and intermodulation current peaks. The larger peaks were used to calculate the corrosion current. The inhibition efficiencies, % IE calculated from Eq. (3) increase with increasing the studied inhibitor concentrations. The two frequencies may not be chosen at random. They must both be small, integer multiples of a base frequency that determines the length of the experiment. Intermodulation spectra obtained from EFM measurements were constructed for iron 0.6 M H_2NHSO_3 solutions in absence (Fig. 9) and presence of 2×10^{-4} M of compound (*D*) (Fig. 10) at 25˚C. Each spectrum is a current response as a function of frequency, data not shown here. Corrosion kinetic parameters, namely corrosion current density (i_{corr}, Tafel constants (β_a, β_c) and causality factors (CF-2, CF-3), were listed in Table 9 as a function of concentrations of investigated compounds at 25˚C. The causality factors in Table 9, which are very close to theoretical values according to the EFM theory, should guarantee the validity of Tafel slopes and corrosion current densities. The standard values for CF-2 and CF-3 are 2.0 and 3.0, respectively [46].

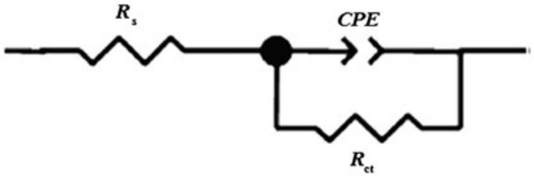

Fig. 8. Electrochemical equivalent circuit used to fit the impedance measurements that include a solution resistance (R_s), a constant phase element (CPE), and a polarization resistance or charge transfer (R_{ct}).

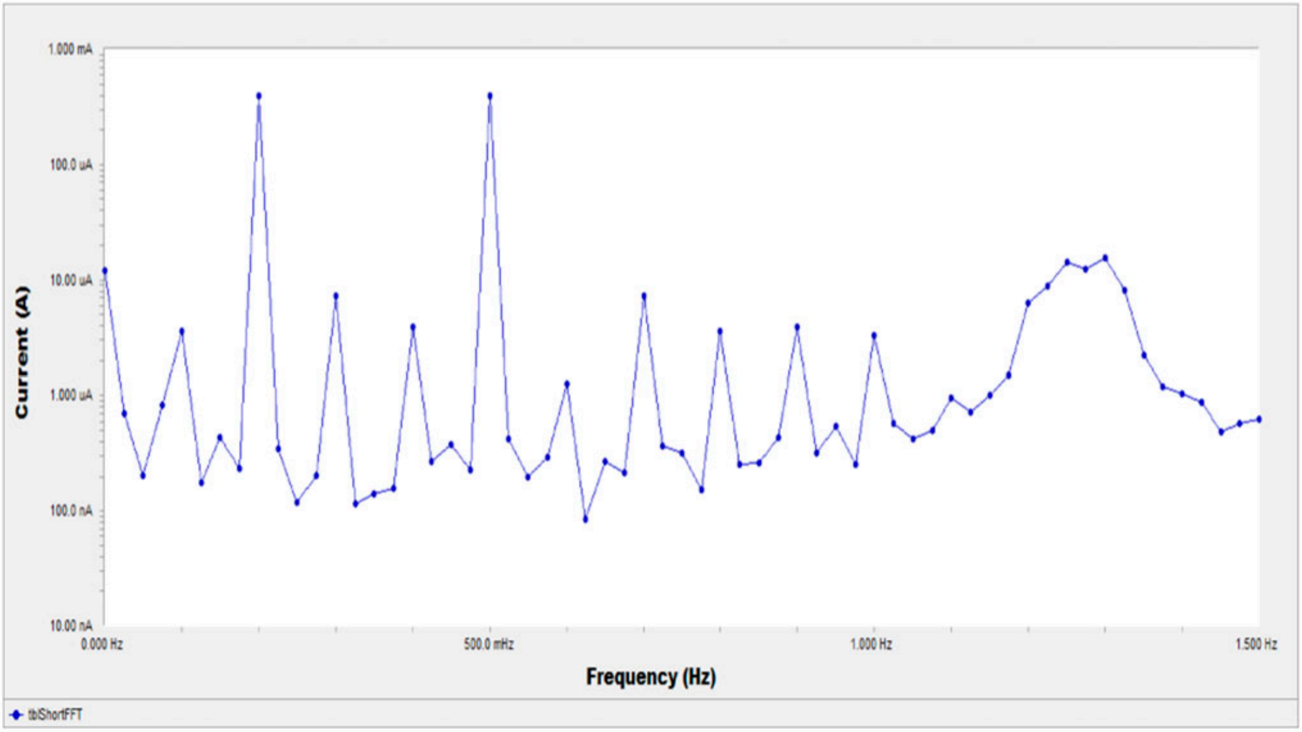

Fig. 9. EFM spectra for 316L SS in 0.6 M H_3NSO_3 (blank).

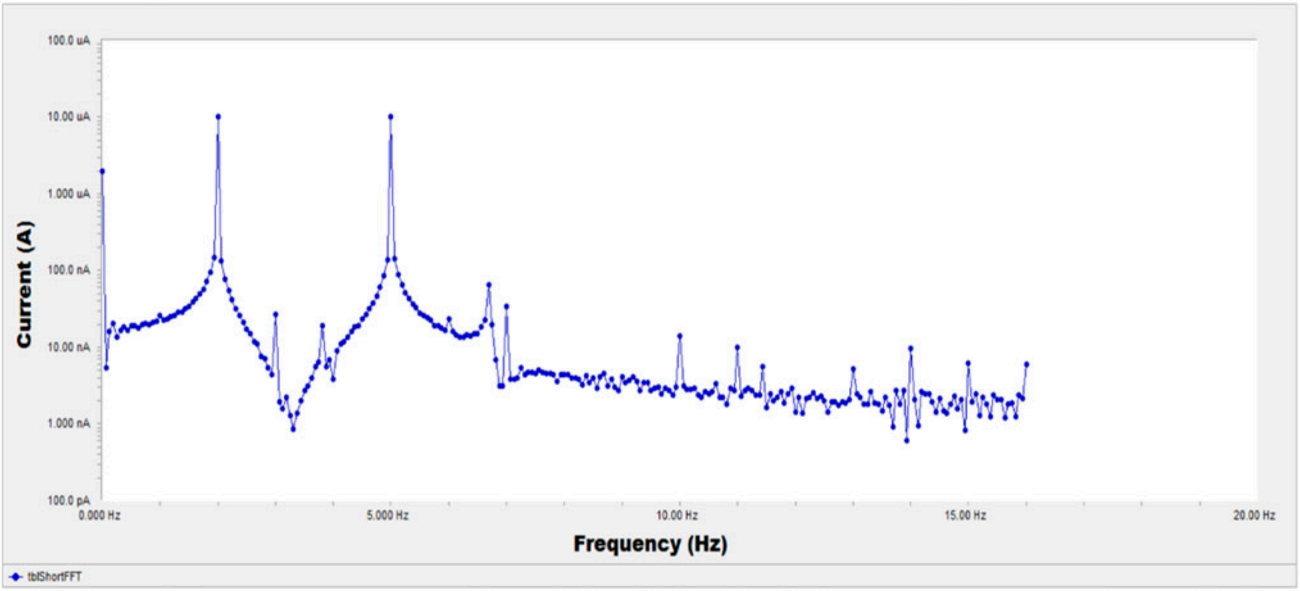

Fig. 10. EFM spectra for 316L SS in 0.6 M H_3NSO_3 in the presence of 2×10^{-4} M inhibitor (*D*).

3.7. Quantum chemical calculation

The quantum chemical method was introduced to study the relationship between the organic molecular structure and the inhibition effect. Four parameters, E_{HOMO}, E_{LUMO}, ΔE ($E_{\mathrm{LUMO}} - E_{\mathrm{HOMO}}$), and μ are listed in Table 10 and the optimized geometry structures of the investigated compounds were in Fig. 11.

Table 9
Electrochemical kinetic parameters obtained from EFM technique for 316L SS in (0.6 M) H_3NSO_3 in the absence and presence of different concentrations of investigated compounds

Inh.	Conc., M	i_{corr}, μA cm^{-2}	β_a, mV dec^{-1}	β_c, mV dec^{-1}	CF-2	CF-3	% IE
Blank	0.0	666.0	104	117	2.012	4.579	–
A	4×10^{-5}	297.3	90	112	1.957	3.000	55.4
	8×10^{-5}	173.9	73	122	2.016	2.872	73.9
	1.2×10^{-4}	145.6	63	126	1.952	2.134	78.1
	1.6×10^{-4}	138.4	72	137	1.973	2.859	79.2
	2×10^{-4}	124.0	81	144	1.973	2.830	81.4
B	4×10^{-5}	275.6	105	140	1.984	3.392	58.6
	8×10^{-5}	161.8	59	136	1.942	3.009	75.7
	1.2×10^{-4}	137.4	62	122	1.898	3.236	79.4
	1.6×10^{-4}	135.4	73	158.4	1.965	2.956	79.7
	2×10^{-4}	116.8	70	155	1.953	2.936	82.5
	4×10^{-5}	322.5	98	116	1.961	2.151	51.6
C	4×10^{-5}	322.5	98	116	1.961	2.151	51.6
	8×10^{-5}	228.2	88	145	1.962	4.086	65.7
	1.2×10^{-4}	164.7	74	136	2.000	2.771	75.3
	1.6×10^{-4}	159.2	85	115	1.981	3.138	76.1
	2×10^{-4}	128.4	68	133	1.966	2.801	80.7
D	4×10^{-5}	214.3	88	110	1.917	2.9	67.8
	8×10^{-5}	144.0	71	126	1.965	2.842	78.4
	1.2×10^{-4}	129.0	74	119	1.981	3.089	80.6
	1.6×10^{-4}	116.0	69	142	1.957	3.183	82.6
	2×10^{-4}	59.36	70	198	3.455	2.75	91.0

It is well known that E_{LUMO} presented the ability of accepting electrons and E_{HOMO} is associated with the electron donating ability of the molecule. Thus, the lower E_{LUMO}, the greater the capability of accepting electrons [47] and high E_{HOMO} were likely to indicate a strong tendency of the molecule to donate electrons to appropriate acceptor molecules with low energy, empty electron orbital such as 3d orbital of Fe atom. ΔE is also an important parameter to indicate the activity of chemical reaction. The higher ΔE, the better stable the substance was.

From Table 10 it can be found that % IE is not only influenced by one factor, such as E_{HOMO}, E_{LUMO}, ΔE, μ or other not mentioned in this paper. All of these indicated that both chemisorption and physisorption might take place at the same time in the adsorption process [48], which is in accordance with the conclusion of thermodynamic calculations (ΔG°_{ads}).

3.8. Mechanism of inhibition

All previous results support that styrylbenzoxazoles derivatives were actually inhibited by the corrosion of 316L SS in sulfamic acid solutions. The corrosion inhibition is due to their physical adsorption and formation of protective film of the adsorbate on the 316L SS surface.

The inhibitive effect of oxazole derivatives may be attributed to the accumulation of the inhibitor molecules on to the metal surface, which reduces the direct contact of the metal with the corrosive environment. It is previously reported that in aqueous acid solutions, the surface of 316L SS samples is positively charged [49,50]. The styrylbenzoxazoles derivatives may be adsorbed on the positively charged surface in the form of neutral molecules, involving displacement of water molecules from the metal surface and sharing electrons between nitrogen and oxygen atoms and the metal surface [51].

Furthermore, adsorption can occur via adsorbed anion $SO_3NH_2^-$ at the positively charged 316L SS surface. The adsorbed $SO_3NH_2^-$ anion makes a negatively charged double layer and consequently it results in an

Table 10
Quantum chemical parameters for the investigated compounds

Comp.	$-E_{HOMO}$,eV	$-E_{LUMO}$, eV	ΔE_{gap},eV	μ, (Debye)
A	8.991	1.462	7.529	3.765
B	8.943	1.43	7.513	3.757
C	9.158	1.299	7.859	3.930
D	8.599	1.44	7.159	3.580

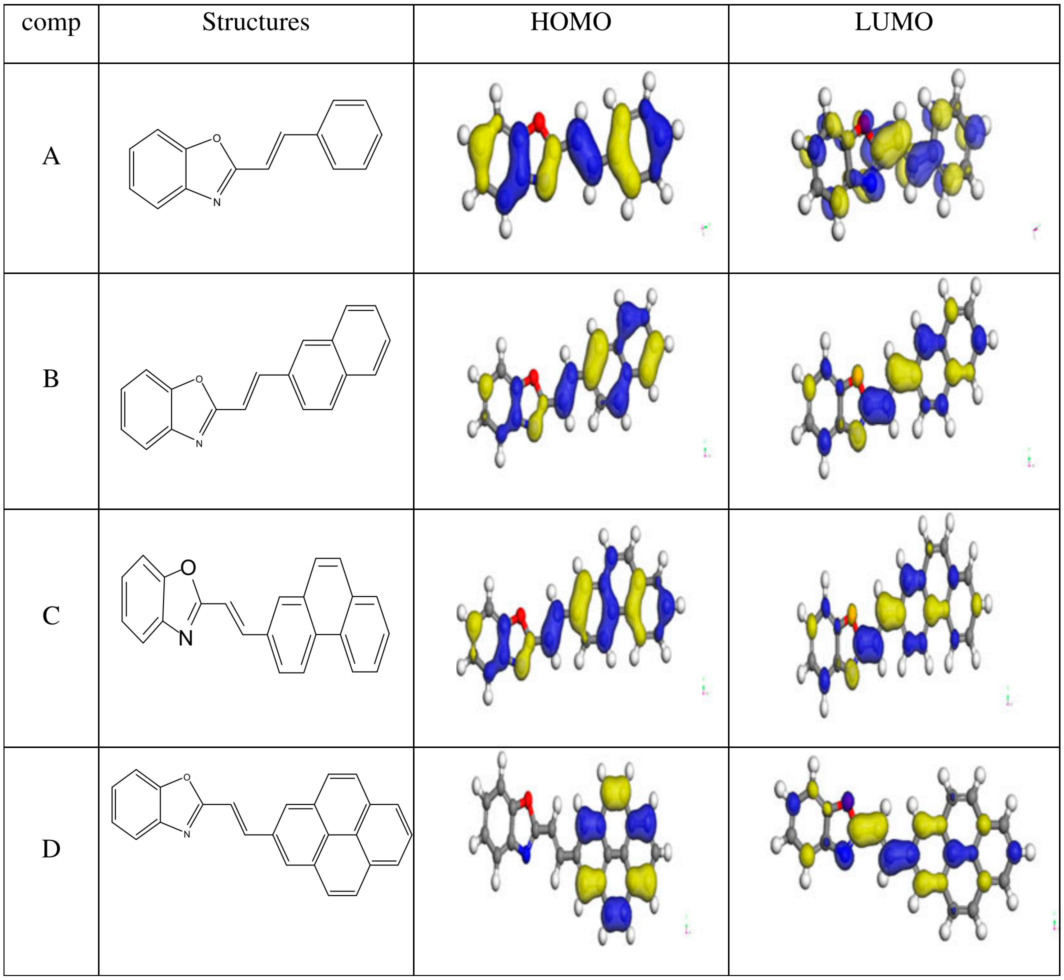

Fig. 11. Molecular structure and frontier molecule orbital density distribution of the studied compounds.

increase in the adsorption capability of the neutral oxazole derivatives effect arises. The order of inhibition efficiency is as follows: D > B > A > C.

Compound (D) exhibits very good inhibition efficiency, probably because of the presence of nitrogen and oxygen atoms as well as the presence of five aromatic rings in the molecule and in other hand it has the highest molecular size. This molecule may be adsorbed flat on SS surface, so it covers more surface area, and hence more inhibition efficiency was obtained. Compound (B) comes after compound (D) in inhibition efficiency due to it contains one nitrogen and one oxygen and three aromatic rings and it has less molecular size. Compound (A) comes after compound (B) in order of inhibition efficiency this is due to it has less molecular size and contains one nitrogen, one oxygen atom, and only two aromatic rings. Compound (C) is the least one in inhibition efficiency in spite of it has one nitrogen, one oxygen atom, and four aromatic rings this may be the molecule adsorbed vertically on SS surface, so covers less surface area.

4. Conclusions

Styrylbenzoxazoles derivatives act as good inhibitors for the corrosion of 316L SS in 0.6 M H_3NSO_3. The inhibition efficiency of styrylbenzoxazoles derivatives decreased with temperature, which leads to an increase in activation energy of corrosion process. The adsorption of styrylbenzoxazoles derivatives follows Langmuir's adsorption isotherm. The adsorption process is spontaneous and exothermic, accompanied by an increase in entropy. Potentiodynamic polarization curves reveal that styrylbenzoxazoles derivatives are mixed-type inhibitors. The results obtained from different experimental studies are in good agreement.

References

[1] A.U. Malik, I.N. Andijani, N.A. Siddiqi, S. Ahmed, A.S., Studies on the Role of Sulfamic Acid as a Descalant in Desalination Plants, Technical Report No. SWCCRDC-32 in December, Al-Jubal KSA, 1993.

[2] Encyclopedia of Chemical Technology, vol. 21, Sulfamic Acid, Wiley Interscience Publication, New York, NY, 1983, pp. 951–957.

[3] Testing of Metals for the Process Industries, NACE Publication, London, 1986, pp. 267–268.

[4] Metal hand book, corrosion, specific industries and environments, Am. Soc. Metals 13 (1987) 1140–1144.

[5] S.A.M. Refaey, F. Taha, A.M. Abd El-Malak, Corrosion and inhibition of 316L SS in neutral medium by 2-mercaptobenzimidazole, Int. J. Electrochem. Sci. 1 (2006) 80–91.

[6] J. Sun, C.G. Yan, Y. Han, Synthesis of benzofuranofuran derivatives: Model of natural products, Synth Commun. 31 (1) (2001) 151–154.

[7] E. Szocs, G.Y. Vastag, A. Shaban, E. Kalman, Electrochemical behavior of an inhibitor film formed on copper surface, Corros. Sci. 47 (2005) 893–908.

[8] R. Subramanian, V. Lakshminarayanan, Effect of adsorption of some azoles on copper passivation in alkaline medium, Corros. Sci. 44 (2002) 535–554.

[9] S. Ramesh, S. Rajeswari, Evaluation of inhibitors and biocide on the corrosion control of copper in neutral aqueous environment, Corros. Sci. 47 (2005) 151–169.

[10] M.M. El-Naggar, Bis-aminoazoles corrosion inhibitors for copper in 4.0 M HNO_3 solutions, Corros. Sci. 42 (2002) 773–784.

[11] D. Zhong, L. Gao, G. Zhou, Inhibition of copper corrosion in aerated hydrochloric acid solution by heterocyclic compounds containing a mercapto group, Corros. Sci. 46 (2004) 3031–3040.

[12] J. Baartly, N. Huynh, S.E. Bottle, H. Flitt, T. Notoya, D.P. Schweinsberg, Computer simulation of the corrosion inhibition of copper in acidic solution by alkyl esters of 5-carboxybenzotriazole, Corros. Sci. 45 (2003) 81–96.

[13] J.M. Bastidas, P. Pinilla, E. Cano, J.L. Polo, S. Miguel, Copper corrosion inhibition by triphenylmethane derivatives in sulphuric acid media, Corros. Sci. 45 (2003) 427–449.

[14] N. Huynh, S.E. Bottle, T. Notoya, D.P. Schweinsberg, Inhibition of copper corrosion by coatings of alkyl esters of carboxybenzotriazole, Corros. Sci. 44 (2002) 2583–2596.

[15] G. Moretti, F. Guidi, Tryptophan as copper corrosion inhibitor in 0.5 M aerated sulfuric acid, Corros. Sci. 44 (2002) 1995–2011.

[16] Z. Szklarska–Smialowska, M. Kaminski, Effect of various substituents in thiophene on the inhibitor efficiency, Corros. Sci. 13 (1973) 1–10.

[17] J.D. Talai, D.K. Gandhi, *N*-heterocyclic compounds as corrosion inhibitors for aluminum-copper alloy in hydrochloric acid, Corros. Sci. 23 (1983) 1315–1332.

[18] A.S. Fouda, Influence of some thiophene derivatives on the corrosion of iron in nitric acid solution, Monatsh. Chem. 117 (1986) 159–165.

[19] O.O. Adeyemi, C. Singh, Investigation of Anthocleista djalonensis stem bark extract as corrosion inhibitor for aluminum, Pac. J. Sci. Technol. 11 (2) (2010) 455–462.

[20] A.S. Fouda, A. M.Eldesoky, M.A. Elmorsi, M.Y. El sheik, I.A. El said, Benzamide, acetamide and acrylamide as corrosion inhibitors for carbon steel in hydrochloric acid solutions, Int. J. Adv. Res. 2(2) (2014) 4–24.

[21] B. Mernari, L. El Kadi, S. Kertit, 2,5-bis(2-thienyl)-1,3,4-oxadiazole as new corrosion inhibitor of mild steel in acidic média, Bull. Electrochem. 17 (2001) 115–120.

[22] M. Bouklah, B. Hammouti, A. Aouniti, T. Benhadda, Thiophene derivatives as effective inhibitors for the corrosion of steel in 0.5 M H_2SO_4, Prog. Org. Coat. 49 (2004) 225–228.

[23] A. Galal, N.F. Atta, M.H. Hassan, Effect of some thiophene derivatives on the electrochemical behavior of 316L SS in acidic solutions containing chloride ions: II. Effect of temperature and surface studies, Mater. Chem. Phys. 89 (2005) 28–37.

[24] K.F. Khaled, Evaluation of electrochemical frequency modulation as a new technique for monitoring corrosion and corrosion inhibition of carbon steel in perchloric acid using hydrazine carbodithioic acid derivatives, J. Appl. Electrochem. 39 (2009) 429–438.

[25] M. Sahin, S. Bilgic, H. Ylmaz, The inhibition effects of some cyclic nitrogen compounds on the corrosion of the steel in NaCl mediums, Appl. Surf. Sci. 195 (2002) 1–7.

[26] A. Zaafarany, M. Abdallah, Ethoxylated Fatty Amide as corrosion inhibitors for carbon steel in hydrochloric acid solution, Int. J. Electrochem. Sci. 5 (2010) 18–28.

[27] A. Tahghighi, M.M. Heravi, F. Kobarfard, Comparison of the basic strength of solid catalysts in the synthesis of 2-styrylbenzoxazoles under microwave, ultrasonic irradiations and solvent free conditions, Chem. Sci. Trans. 3 (1) (2014) 55–60.

[28] P.O. Ameh, N.O. Eddy, Commiphora pedunculata gum as a green inhibitor for the corrosion of aluminium alloy in 0.1 M HCl, Res. Chem. Intermed. 8(2) (2014) 37–46.

[29] A. Petchiammal, R.P. Deepa, S. Selvaraj, K. Kalirajan, Corrosion protection of Zn in natural sea water using citrullus vulgaris peel as an inhibitor. Res. J. Chem. Sci. 2(4) (2012) 24–34.

[30] A.S. Fouda, A.A. Al-Sarawy, E.E. El-Katori, Pyrazolone derivatives as corrosion inhibitors for Carbon steel in hydrochloric acid solution, Desalination 201 (2006) 1–13.

[31] G. Gece, The use of quantum chemical methods in corrosion inhibitor studies, Corros. Sci. 50(2008) 2981–2992.

[32] L. Tang, X. Lie, Y. Si, G. Mu, G. Liu, The synergistic inhibition between 8-hydroxyl quinoline and chloride ion for the corrosion of cold rolled steel in 0.5 M sulfuric acid, Mater. Chem. Phys. 95 (2006) 29–38.

[33] L. Tang, G. Murad, G. Liu, The effect of neutral red on the corrosion inhibition of cold rolled steel in 1.0 M hydrochloric acid, Corros. Sci. 45 (2003) 2251–2262.

[34] I.N. Putilova, S.A. Balzin, V.P. Barannik, Metallic corrosion Inhibitors, Pergamomon Press, New York, NY, 1960, p. 31.

[35] E. Khamis, Effect of temperature on the acidic dissolution of steel in the presence of inhibitors, Corrosion (NACE) 46 (1990) 476–484.

[36] X. Li, L. Tang, Synergistic inhibition between OP and NaCl on the corrosion of cold-rolled steel in phosphoric acid, Mater. Chem. Phys. 90 (2005) 286–297.

[37] A.A. El-Awady, B. Abd El-Nabey S.G. Aziz, Kinetic-thermodynamic and adsorption isotherms analyses for the inhibition of the acid corrosion of steel by cyclic and open-chain amines, Electrochem. Soc. 139 (1992) 2149–2154.

[38] S.S. Abd El-Rehim, H.H. Hassan, M.A. Amin, Corrosion inhibition of aluminum by 1, 1(lauryl amido) propyl ammonium chloride in HCl solution, Mater. Chem. Phys. 70 (2001) 64–72.

[39] A.K. Singh, M.A. Quraishi, The effect of some bis-thiadiazole derivatives on the corrosion of mild steel in hydrochloric acid, Corros. Sci. 52 (2010) 1373–1385.

[40] F. Bentiss, C. Jama, B. Mernari, H.E. Attari, L.E. Kadi, M. Lebrini, M. Traisnel, M. Lagrenee, Corrosion control of mild steel using 3,5-bis(4-methoxyphenyl)-4-amino-1,2,4-triazole in normal hydrochloric acid medium, Corros. Sci. 51 (2009) 1628–1635.

[41] H. Ashassi-Sorkhabi, D. Seifzadeh, M.G. Hosseini, EN, EIS and polarization studies to evaluate the inhibition effect of 3H-phenothiazin-3-one, 7-dimethylamin on mild steel corrosion in 1 M HCl solution, Corros. Sci. 50 (2008) 3363–3370.

[42] A. Popova, M. Christov, Evaluation of impedance measurements on mild steel corrosion in acid media in the presence of heterocyclic compounds, Corros. Sci. 48 (2006) 3208–3221.

[43] Gamry Echem Analyst Manual, Revision 4.2, USA, (2003).

[44] R.W. Bosch, J. Hubrecht, W.F. Bogaerts, B.C. Syrett, A New Electrochemical Technique for Online Corrosion Monitoring, Corrosion (NACE) 57 (2001) 60–70.

[45] S.S. Abdel-Rehim, K.F. Khalid, N.S. Abd-Elshafi, Electrochemical frequency modulation as a new technique for monitoring corrosion inhibition of iron in acid media by new thiourea derivative, Electrochim. Acta 51 (2006) 3269–3277.

[46] A.K. Singh, M.A. Quraishi, Piroxicam; A novel corrosion inhibitor for mild steel corrosion in HCl acid solution, J. Mater. Environ. Sci. 1 (2010) 101–110.

[47] N. Khalil, Quantum chemical approach of corrosion inhibition, Electrochim. Acta 48 (2003) 2635–2640.

[48] W. Li, Q. He, C. Pei, B. Hou, Experimental and theoretical investigation of the adsorption behaviour of new triazole derivatives as inhibitors for mild steel corrosion in acid media, Electrochim. Acta 52 (2007) 6386–6394.

[49] R. Solmaz, G. Kardas, B. Tazc, M. Erbil, Adsorption and corrosion inhibitive properties of 2-amino-5-mercapto-1,3,4-thiadiazole on mild steel in hydrochloric acid media, Colloids. Surf. A 312 (2008) 7–17

[50] M.H. Wahdan, A.A. Hermas, M.S. Morad, Corrosion inhibition of carbon-steels by propargyltriphenylphosphonium bromide in H_2SO_4 solution, Mater. Chem. Phys. 76 (2002) 111–118.

[51] F. Bentiss, M. Traisnel, L. Gengembre, M. Lagrene, A new triazole derivative as inhibitor of the acid corrosion of mild steel: Electrochemical studies, weight loss determination, SEM and XPS, Appl. Surf. Sci. 152 (1999) 237–249.